Journal of Hazardous Materials 165 (2009) 78–86

Contents lists available at ScienceDirect

Journal of Hazardous Materials

journal homepage: www.elsevier.com/locate/jhazmat

Factors influencing the dechlorination of 2,4-dichlorophenol by Ni–Fe nanoparticles in the presence of humic acid

Zhen Zhang[a,b], Naman Cissoko[a], Jingjing Wo[a], Xinhua Xu[a,*]

[a] Department of Environmental Engineering, Zhejiang University, Hangzhou 310027, People's Republic of China
[b] School of Bioscience, Taizhou University, Linhai 317000, People's Republic of China

ARTICLE INFO

Article history:
Received 26 May 2008
Received in revised form 8 September 2008
Accepted 19 September 2008
Available online 27 September 2008

Keywords:
2,4-DCP
Catalytic dechlorination
Ni–Fe nanoparticles
Humic acid
Mechanisms
Kinetics

ABSTRACT

The dechlorination of 2,4-dichlorophenol (2,4-DCP) by Ni–Fe nanoparticles in the presence of humic acid (HA) was investigated to understand the feasibility of using Ni–Fe for the in situ remediation of contaminated groundwater. 2,4-DCP was first adsorbed by Ni–Fe nanoparticles, then quickly reduced to *o*-chlorophenol (*o*-CP), *p*-chlorophenol (*p*-CP), and finally to phenol (P). However, the introduction of HA decreased the removal percentage of 2,4-DCP, as a result, the phenol production rates dropped from 86% (in the absence of HA) to 29% within 2 h. Our data suggested that the dechlorination rate was dependent on a number of factors including Ni–Fe availability, Ni loading percentage over Fe, temperature, pH, and HA concentration. In particular, the removal percentage of 2,4-DCP was determined to be 100, 99, 95, 84 and 69%, for HA concentrations of 0, 5, 10, 30 and 40 mg L^{-1}, respectively. The kinetic calculations for the dechlorination of 2,4-DCP indicated that k values for 2,4-DCP dechlorination dropped from 0.14, 0.051, 0.039, 0.021 to 0.011 min^{-1} with increasing concentrations of HA from 0, 5, 10, 30 to 40 mg L^{-1}.

1. Introduction

Chlorinated organic compounds (COCs) have been so widely used that they can be found in nearly all major environmental compartments. For example, chloroaromatics have a wide range of industrial and domestic uses, and they are employed as industrial solvents or intermediates in the synthesis of other chemicals, dyestuffs, pesticides, lubricants, and dielectric [1]. Chloroaromatics are among the hazardous pollutants found in various waste oils and other organic liquids, and they are highly toxic, mutagenic and possibly carcinogenic. Furthermore, chloroaromatics are biorefractory and tend to accumulate in animal tissues. Once released into the environment, they accumulate in the surroundings and pose health threat to humans and ecosystems over a long period of time [2–5]. This raises an urgent need for efficient dechlorination methods to eliminate chloroaromatics from both concentrated industrial effluents and diluted polluted groundwater.

Recently, chemical reduction of hazardous compounds such as COCs using zero-valent iron (ZVI) has been intensively studied for both in situ and aboveground treatment of contaminated water. Recent study on metal iron technology showed that the use of zero-valent single metals to reduce chlorinated organics has some drawbacks [6–10]. For example, even when nanoscale zero-valent iron particles are used, the metal mass normalized observed rate constant for the dechlorination of trichloroethylene (TCE) is still very low, in the order of 10^{-2} L g^{-1} h^{-1} [11]. More importantly, the formation of a hydroxide or oxide layer on the particle surface, during the reaction or upon contact of the nanoparticles with air, significantly reduced their reactivity and decreased the effective use of the metal particles [12]. Further attempts have been made to enhance the dechlorination rate of COCs using hydrogen gas and noble bimetallic particles such as Ni/Fe, Pd/Fe and Cu/Fe [13–16]. Cheng and Wu [17] reported that the physical addition of Pd^0, Cu^0 or Ni^0 micron-sized powder could re-activate Fe^0 particles that have lost their surface activity. It is well known that the reduction of chlorinated organics by bimetallic particles occurs via hydrodechlorination instead of inter-metalic electron transfer, in which Fe acts as the reducing agent whereas Ni, Pd, or Cu acts as a catalyst. The latter are considered as good hydrogenation catalysts and have a high ability to dissociate H_2 [18]. The presence of a second metal not only increases the reactivity and reduces the accumulation of toxic byproducts, but also inhibits particle oxidation in air [19].

Although the bimetallic system and the nanoscale bimetallic system are effective in contaminant dechlorination, the reactivity of the zero-valent metals is highly controlled by the surface characteristics of metals and groundwater chemistry. In subsurface environments, natural humic substances (HS) such as humic acid (HA) are abundant and play important roles in both electron

* Corresponding author. Tel.: +86 571 87951239; fax: +86 571 87952771.
E-mail address: xuxinhua@zju.edu.cn (X. Xu).

0304-3894/$ – see front matter © 2008 Published by Elsevier B.V.
doi:10.1016/j.jhazmat.2008.09.080

transfer and adsorption processes. The inhibition of chlorinated hydrocarbons dechlorination by zero-valent metals in the presence of natural HS was reported by Johnson et al. [20]. They depicted that any non-reactive adsorbates that out-compete the contaminants for reactive surface sites would result in decreased degradation rate. Tratnyek et al. found that the reduction rate of TCE by ZVI was inhibited by natural HS due to the competitive sorption onto the surface of ZVI [21]. However, HA also can act as an electron mediator to enhance the reduction efficiency of chlorinated aliphatic compounds in aqueous solutions containing bulk reductant and to facilitate the microbially mediated anaerobic dechlorination of chlorinated hydrocarbons under iron-reducing conditions [22,23]. So far, it is not clear whether HA enhances or inhibits the electron transfer process from a bimetallic system such as Ni–Fe to the target compounds during in situ treatment processes. Therefore, knowledge of the role of HA in the dechlorination of chlorinated hydrocarbons is thus required prior to applying it for in situ remediation treatment [24].

To evaluate the performance of the bimetallic systems in the remediation of contaminated groundwater under ambient condition, the role of HA in the dechlorination of 2,4-DCP by nanoscale Ni–Fe particles was investigated in this study. In addition, other factors contributing to 2,4-DCP reduction, such as Ni–Fe nanoparticles dosage, Ni content, initial 2,4-DCP concentration, initial pH values and temperature, were examined.

2. Experimental

2.1. Chemicals

Nickel sulfate hexahydrate, iron sulfate heptahydrate, 2,4-DCP, *o*-CP, *p*-CP, phenol (P) and other reagents were purchased from Sinopharm Group Chemical Reagent Co., Ltd., China, and used as received without further purification. HA was obtained from Sigma–Aldrich (ash ~ 20%, Switzerland). A HA stock solution (500 mg L^{-1}) was prepared by dissolving 0.25 g of HA in 2 mL of a 0.1 M NaOH aqueous solution, followed by sonication, dilution with deionized water to 500 mL, the final pH of the solution was adjusted to 7. The solution was then filtered through a 0.45 μm pore diameter Millipore membrane to remove the insoluble solids, and stored at 4 °C before use. 2,4-DCP is dissolved in deionized water and stored at 4 °C. The nanoscale Fe^0 and Ni–Fe were synthesized immediately before use.

2.2. Synthesis procedure

Ni–Fe nanoparticles were prepared in a 1000 mL three-necked flask under nitrogen gas. The iron nanoparticles were synthesized by dropwise addition of stoichiometric amounts of $NaBH_4$ aqueous solution into the flask containing $FeSO_4{\cdot}7H_2O$ aqueous solution simultaneously with electrical stirring at 25 °C. The ferrous iron was reduced to zero-valent iron according to the following reaction:

$$Fe(H_2O)_6^{2+} + 2BH_4^- \rightarrow Fe^0 + 2B(OH)_3 + 7H_2 \quad (1)$$

The Fe^0 nanoparticles were then rinsed several times with deionized water. Subsequently, the nanoparticles were prepared by the reaction of the wet Fe^0 nanoparticles with an aqueous solution of nickel sulfate hexahydrate under stirring according to the following equation:

$$Fe^0 + Ni^{2+} \rightarrow Fe^{2+} + Ni \quad (2)$$

The nanoparticles were then rinsed with deionized water to remove excess SO_4^{2-} ions.

2.3. Batch experimental procedures

The batch experiments for 2,4-DCP dechlorination in the presence of HA were performed in the same three-necked flask into which 3.0 g Ni–Fe nanoparticles were added. The benchmark experiment conditions were as following: 5 mL 1.0 g L^{-1} HA, 10 mL 1.0 g L^{-1} 2,4-DCP stock solution and a certain amount of deoxygenated deionized water were added into the flask containing freshly prepared nanoscale Ni–Fe particles, total reaction volume was 500 mL. The reaction solution was stirred under nitrogen flow to simulate anaerobic environment in groundwater in 25 °C, and the initial pH was 5.7, the hydraulic retention time were 2 h. Samples were periodically collected in 0, 10, 30, 60, 90, and 120 min with glass syringes and the reaction was stopped by passing the aliquots through 0.22 μm membrane filters, then analyzed in 4 h. Condition experiments were conducted under the benchmark experiment conditions except the change in corresponding conditions.

2.4. Analyses procedures

Fresh metal particles (with a Ni bulk loading of 2.0%) were visualized under a JEOL JEM 200CX transmission electron microscope (TEM) at 160 kV for morphological measurements. Prior to TEM analysis, the particles immersed in deionized water were dispersed by an ultrasonicator.

Organic compounds such as 2,4-DCP, *p*-CP, *o*-CP and phenol were measured by SHIMADZU High Performance Liquid Chromatography [25]. Agilent TC-C18 Column, 150 × 4.6. Mobile phase: MeOH/H_2O (60/40, v/v), flow rate: 1.0 mL min^{-1}, detector: UV at 280 nm, sample size: 20 μL.

3. Results and discussion

3.1. Inhibition by humic acid

Catalytic dechlorination of 2,4-DCP over Ni–Fe nanoparticles with and without 40 mg L^{-1} HA is shown in Fig. 1. 2,4-DCP was first adsorbed by the nanoparticles then reduced to *o*-CP or *p*-CP, and later converted to phenol, phenol was the sole final organic product. No other chlorinated intermediates or final organic products were detected.

The concentration of 2,4-DCP decreased rapidly and the removal percentage reached 99% in 30 min, then reached 100% in 120 min for Ni–Fe nanoscale particles in the absence of HA. In contrast, only about 50% and 69% of removal percentage was obtained in the presence of 40 mg L^{-1} HA in 30 and 120 min, respectively. And the concentration of *p*-CP remained low during the whole reaction with or without the addition of 40 mg L^{-1} HA. As for *o*-CP, it is the concentration peaked at 10 min in the absence of HA. The addition of 40 mg L^{-1} HA made the removal of 2,4-DCP slowed down, and *o*-CP peaked at 30 min. Meanwhile, the addition of 40 mg L^{-1} HA lowered the production rate of phenol, which was expressed as the ratio of the actual amount of phenol produced to the theoretical amount of phenol during the total dechlorination of 2,4-DCP, from 86% in the absence of HA to 29% in 2 h. Phenol and inorganic chlorine were detected as final products. Compared to initial concentration (20 mg L^{-1}), approximately 15% mass loss was observed. This suggests that a fraction of organic compounds was absorbed or covered by surface passivating layers, most likely due to the precipitation of metal hydroxides and metal carbonates on the surface of iron and Ni–Fe particles for their large surface areas. This is also evidenced by that the 2,4-DCP concentration dropped rapidly in the first 10 min, but the phenol generated was much less than the maximum attainable. The non-detected fraction of intermediates may be attributed to the fact that the high surface area to volume ratios

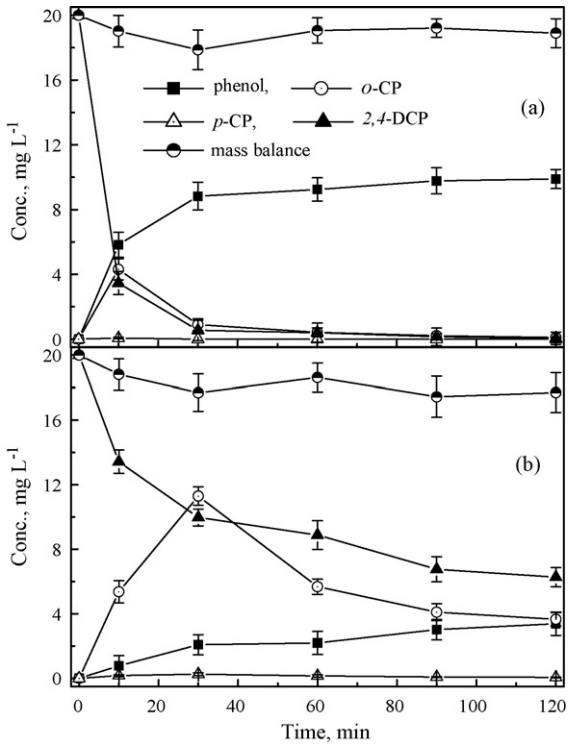

Fig. 1. Dechlorination of 2,4-DCP and distribution of products by Ni–Fe nanoparticles (a) in the absence and (b) presence of 40 mg L^{-1} humic acid (T: 25 °C, pH_{in}: 5.7, $C_{2,4\text{-DCP}}$: 20 mg L^{-1}, C_{Ni-Fe}: 6 g L^{-1}, stirring rate: 400 rpm, the nickel content: 2.0 wt%).

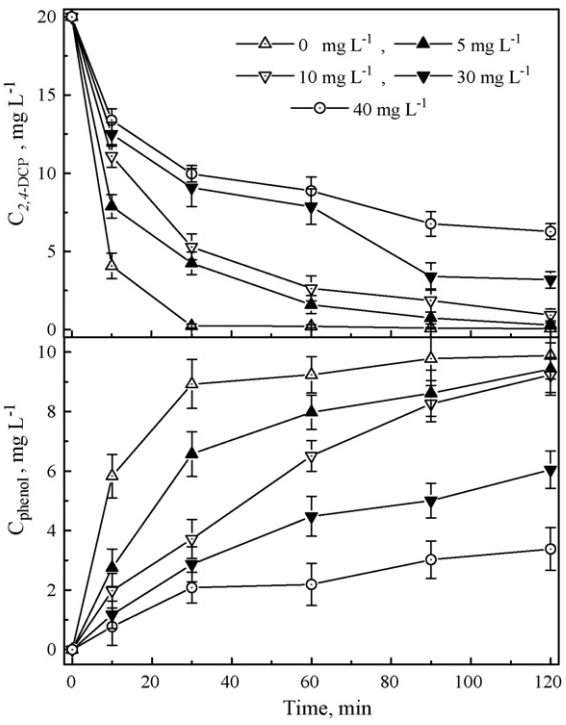

Fig. 2. Effect of humic acid on 2,4-DCP dechlorination by nanoscale Ni–Fe particles (T: 25 °C, pH_{in}: 5.7, $C_{2,4\text{-DCP}}$: 20 mg L^{-1}, C_{Ni-Fe}: 6 g L^{-1}, stirring at 400 rpm, the nickel content was 2.0 wt%).

of nanoscale Ni–Fe that appear to serve as non-reactive sorption sites for intermediates [26].

3.2. The effect of humic acid on 2,4-DCP dechlorination

The concentration effect of HA on the dechlorination of 2,4-DCP by Ni–Fe was further examined. Fig. 2 illustrates the dechlorination of 2,4-DCP by Ni–Fe at various concentrations of HA ranging from 0 to 40 mg L^{-1}. The HA concentration increased from 0, 5, 10, 30 to 40 mg L^{-1} led to the decrease in 2,4-DCP removal percentages from 100, 99, 95, 84 to 69% in 120 min, and this trend was indeed more obvious at much lower HA concentrations. Meanwhile the production rates of phenol dropped from 86, 80, 80, 52 to 29%, respectively. The decrease of both 2,4-DCP removal percentages and phenol production rates with increasing HA concentrations suggest that the existence of HA has a significant impact on 2,4-DCP dechlorination efficiency.

Several hypotheses were tested to identify mechanisms behind these scenarios. The accumulation of adsorbed HA on the nanoscale Ni–Fe surface may reduce the 2,4-DCP reduction rate. The complexation between HA and the generated Fe(II) may inhibit 2,4-DCP reduction by Fe(II) or occupy the active surface sites and inhibit iron corrosion. On the other hand, excavation of active surface sites by dissolution of passive iron oxides may accelerate the 2,4-DCP reduction. The redox-active moieties in HA or in Ni–Fe–HA complexes may act as reductants to reduce 2,4-DCP to phenol or serve as electron-transfer mediators between Ni–Fe and 2,4-DCP [27].

Considering the 2,4-DCP reduction (Fig. 2), it may be concluded that HA effects may be limited by insufficient reaction time when added simultaneously with 2,4-DCP. However, in the long run, the amount of humic acid adsorbed on the Ni–Fe surface may increase, while the 2,4-DCP is continuously reduced, and this may eventually affect the 2,4-DCP reduction.

On the other hand, after a certain decrease in the initial 2,4-DCP concentration, the reaction becomes retarded and the onset of the "slowing down" seems to depend on the initial HA loading. It is hypothesized that the similarity in initial rates caused by existence of specific active surface sites designated for 2,4-DCP reduction, not for HA adsorption; with the reactions proceeding to exhaust those specific sites, the common active sites (available for both 2,4-DCP reduction and HA adsorption) become limited. The adsorption of HA on the Ni–Fe surface led to large changes in the later reaction.

Ferrous ions and total iron ions can also be detected since the redox reaction took place in an aqueous solution. Considerating the mass balance, ferrous ions and total iron ions in solution must come from the corrosion of Ni–Fe nanoparticles. Fig. 3 shows the concentration change of ferrous ions and total iron ions in solution during the reaction. Both of the concentration of ferrous ions and total iron ions increased in initial 30 min, and then decreased slowly.

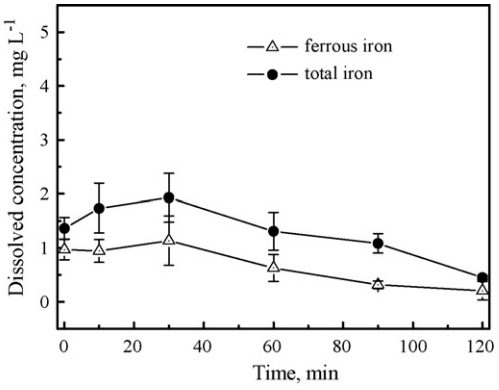

Fig. 3. Concentration changes of ferrous ions and total iron ions in solution (T: 25 °C, pH_{in}: 5.7, $C_{2,4\text{-DCP}}$: 20 mg L^{-1}, C_{HA}: 10 mg L^{-1}, C_{Ni-Fe}: 6 g L^{-1}, stirring at 400 rpm, the nickel content was 2.0 wt%).

During the whole reaction the concentration of ferrous ions were no more than 1.5 mg L^{-1}, and the total iron ions were no more than 2.5 mg L^{-1}. It indicates that the corrosion of Ni–Fe indeed existed during the reduction course of 2,4-DCP dechlorination by Ni–Fe nanoparticles. And it is in good agreement with the study of Lu et al. [28]. This phenomenon will be further discussed in greater detail later.

3.3. Effect of initial pH values on 2,4-DCP dechlorination in the presence of HA

The solution pH value is important in reductive dechlorination of chlorinated organic compounds using ZVI [29]. Low pH favors more iron surface available for reaction with the chlorinated molecules or at least promote the corrosion rate, leading to the release of chloride ions. However, when oxygen was present in the reaction solution, the corrosion product, OH^-, was generated. Therefore, the solution pH should increase even if the initial pH is low. At higher pH values, carbonate and hydroxide coatings undoubtedly develop, which inhibit further decomposition of iron surface and hinder access to the Fe^0 surface [30,31]. As a result, the catalyst activity decreases. Fig. 4 shows the effect of different initial pH values on the dechlorination of 2,4-DCP by Ni–Fe nanoparticles in the presence of the HA. Prior to initializing reaction all reactant solutions were adjusted to different pH values by diluted sulfuric acid (H_2SO_4) and sodium hydroxide (NaOH), and during the reaction pH values were not adjusted. When the initial pH values increased from 3, 6, 8, 9 to 11, the removal percentages of 2,4-DCP dropped from nearly 100, 95, 69, 48 to 46% in 120 min, while the production rates of phenol dropped from 84, 80, 41, 33 to 30%; also the removal percentages of 2,4-DCP were found consistently higher than the production rates of phenol, respectively. The increase of initial pH values of the reactant solutions from 6 to 8, leads to the reactant solution change from acidic to alkaline condition, consequently both the removal percentages of 2,4-DCP and the production rates of phenol dropped obviously. It indicates that the presence of H^+ largely enhances the 2,4-DCP reduction even though in the presence of HA. The possible reasons may be that (1) the surface of Ni–Fe particles would be oxidized inevitably during the preparation and storage, which had been demonstrated by the literatures [32]. However, at lower pH values, the oxides on the particles surface were dissolved, and the active sites of the particle surface were exposed; (2) at lower pH values, the iron corrosion could be accelerated, producing enough hydrogen (or hydrogen atoms), which were in favor of hydrogenation reaction [33,34]. (3) Iron corrosion in solution of pH higher than 7 tends to form a passive film of iron oxides and hydroxide on the iron surface, which inhibits further reaction.

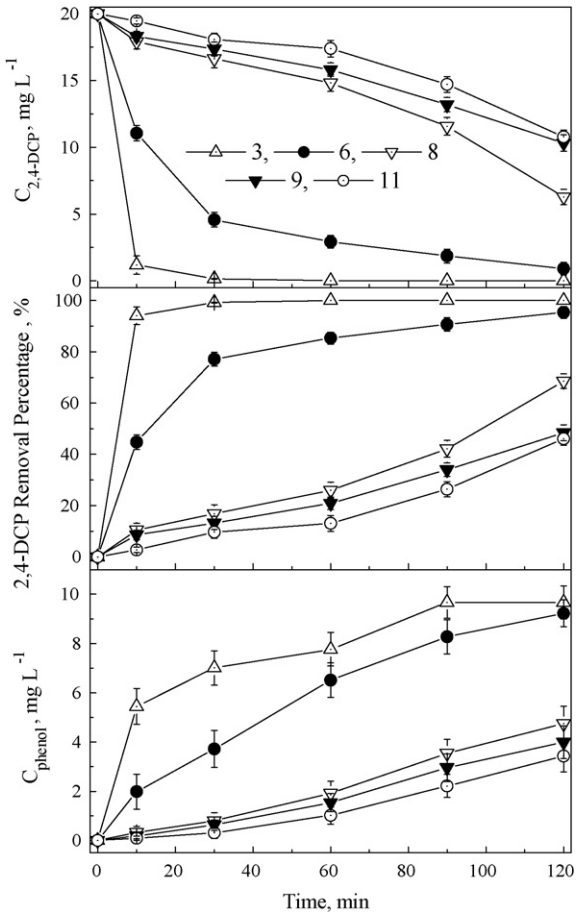

Fig. 4. Effect of pH values on 2,4-DCP dechlorination by nanoscale Ni–Fe nanoparticles (T: 25 °C, $C_{2,4\text{-DCP}}$: 20 mg L^{-1}, C_{HA}: 10 mg L^{-1}, C_{Ni-Fe}: 6 g L^{-1}, stirring at 400 rpm, the nickel content was 2.0 wt%).

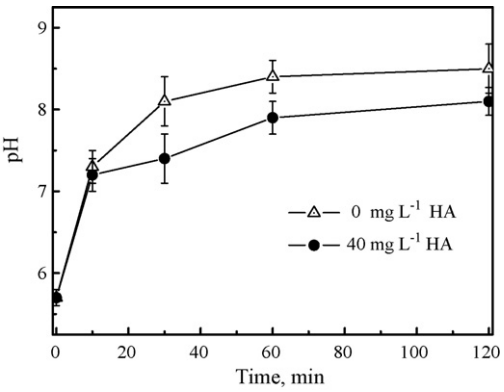

Fig. 5. pH change during the entire period of the reaction in the absence and presence of 40 mg L^{-1} humic acid (T: 25 °C, pH_{in}: 5.7, $C_{2,4\text{-DCP}}$: 20 mg L^{-1}, C_{Ni-Fe}: 6 g L^{-1}, stirring at 400 rpm, the nickel content was 2.0 wt%).

The solution pH was monitored during the entire period of the reaction. As shown in Fig. 5, the solution pH increased sharply to around 7.3 in the first 10 min, then gradually increased to 8.5 in 60 min in the absence of HA and 8.1 in the presence of 40 mg L^{-1} HA when the initial pH was 5.7. In the presence of 40 mg L^{-1} HA the final pH was a little lower than that in the absence of HA, it indicates that HA has some buffering effect on the solution pH. Presumably, the iron corrosion is the rate limited reaction under the experimental condition of the present study. Therefore, detection of ferrous ions and total iron ions produced in the reaction, which were shown in Fig. 3, could support our assumption.

3.4. Effects of Ni–Fe nanoscale particles dosage on 2,4-DCP dechlorination in the presence of HA

Since the reductive dechlorination by Ni–Fe nanoscale particles takes place on the surface of particles, the Ni–Fe-to-2,4-DCP ratio (g Ni–Fe/mg 2,4-DCP) is also a significant variable parameter. The quantity of available surface area is among the most significant experimental variables affecting contaminant reduction. Increasing the concentration of Ni–Fe nanoscale particles in the solution, insignificant to the final removal efficiency in excess of Ni–Fe dosage, will accelerate the initial reaction rate and provide more active sites of Ni–Fe nanoscale particles for collision with 2,4-DCP during the reduction. Different Ni–Fe nanoscale particles dosages of 2, 4, 6 and 8 g L^{-1} were evaluated as shown in Fig. 6.

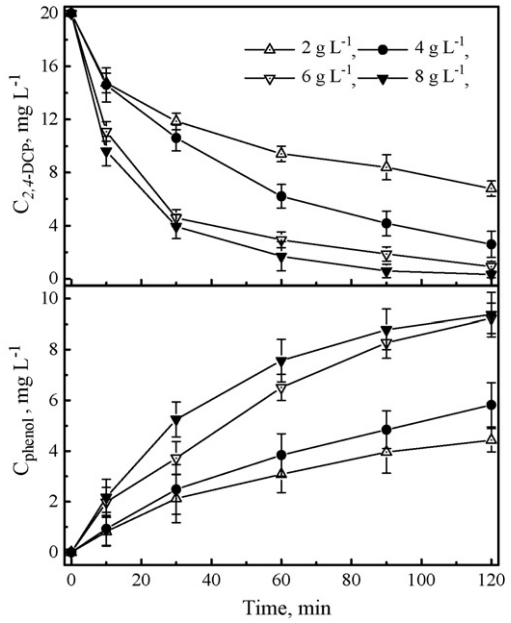

Fig. 6. Effect of Ni–Fe nanoscale particles dosage on 2,4-DCP dechlorination in the presence of HA (T = 25 °C, pH_{in} = 5.7, $C_{2,4\text{-DCP}}$ = 20 mg L^{-1}, C_{HA} = 10 mg L^{-1}, stirring at 400 rpm, the nickel content was 2.0 wt%).

With the elevation of the Ni–Fe nanoscale particles dosage from 2 to 6 g L^{-1}, obvious differences were observed, the removal percentage of 2,4-DCP increased from 69 to 96% after 120 min of the reaction. Increasing the dosage of nanoscale Ni–Fe means the larger Ni–Fe surface area. The higher the Ni–Fe surface area concentration is, the faster the reaction velocity. The removal percentage of 2,4-DCP is similar for a dosage of nanoscale Ni–Fe of 6 or 8 g L^{-1}. Hence, the appropriate dosage of Ni–Fe in the level of 6 g L^{-1} is chosen for 2,4-DCP dechlorination.

3.5. Effects of Ni content on 2,4-DCP dechlorination in the presence of humic acid

It has been elucidated that zero-valent iron can promote a hydrogenolysis reaction where a chlorine in the organic chlorinated compounds is replaced by a hydrogen atom. Nickel is a well-known excellent catalyst for the hydrogenolysis. Co-existence of nickel and iron in the particles has been proved to be very effective to accelerate the dechlorination. Therefore, the content of nickel in the Ni–Fe particles may be one of the important factors in influencing dechlorination efficiency. As shown in Fig. 7, the efficiencies of dechlorination and phenol formations were increased significantly as nickel content increased from 0.5 to 3.0 wt%. The removal percentage of 2,4-DCP reached from 47% to 98% within 120 min. Correspondingly, the production rate of phenol increased from 16% to 92%. The increase in the nickel content from 1.5 to 3.0 wt% caused only slight improvement in the dechlorination efficiency, and the removal percentages of 2,4-DCP within 2 h were maintained higher than 98%. The nickel content was selected at about 2.0 wt% for efficient dechlorination and yet minimal nickel usage.

3.6. Effect of 2,4-DCP initial concentration on 2,4-DCP dechlorination in the presence of HA

Six different initial 2,4-DCP concentrations (60, 50, 40, 30, 20 and 10 mg L^{-1}) were employed. The 2,4-DCP reduction profiles with different initial 2,4-DCP concentrations and fixed 6 g L^{-1} Ni–Fe nanoscale particles content in initial pH value were shown in Fig. 8.

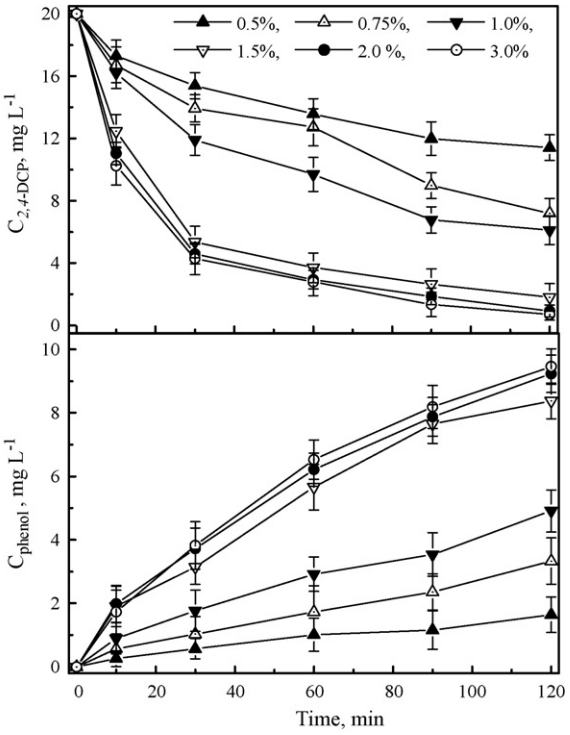

Fig. 7. Effects of Ni content on 2,4-DCP dechlorination by nanoscale Ni–Fe (T: 25 °C, pH_{in}: 5.7, $C_{2,4\text{-DCP}}$: 20 mg L^{-1}, C_{HA}: 10 mg L^{-1}, $C_{Ni\text{–}Fe}$: 6 g L^{-1}, stirring at 400 rpm).

The removal percentages of 2,4-DCP reached 78, 74, 79, 84, 77 and 95% each after 30 min, and then reached 98, 98, 98, 97, 95 and 100% respectively after 2 h of the reaction. Though the final removal percentage of 2,4-DCP was close to each other, the absolute removal amount increased with increasing initial 2,4-DCP concentrations.

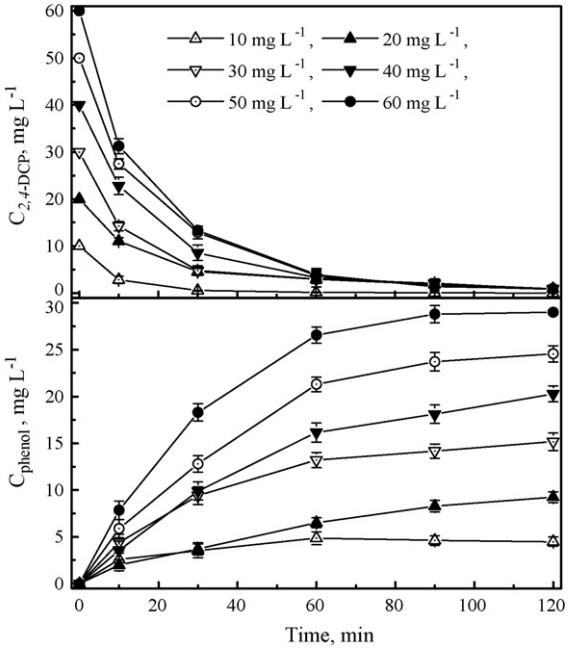

Fig. 8. Effect of initial 2,4-DCP concentration on dechlorination in the presence of humic acid (T: 25 °C, pH_{in}: 5.7, C_{HA}: 10 mg L^{-1}, $C_{Ni\text{–}Fe}$: 6 g L^{-1}, stirring at 400 rpm, the nickel content was 2.0 wt%).

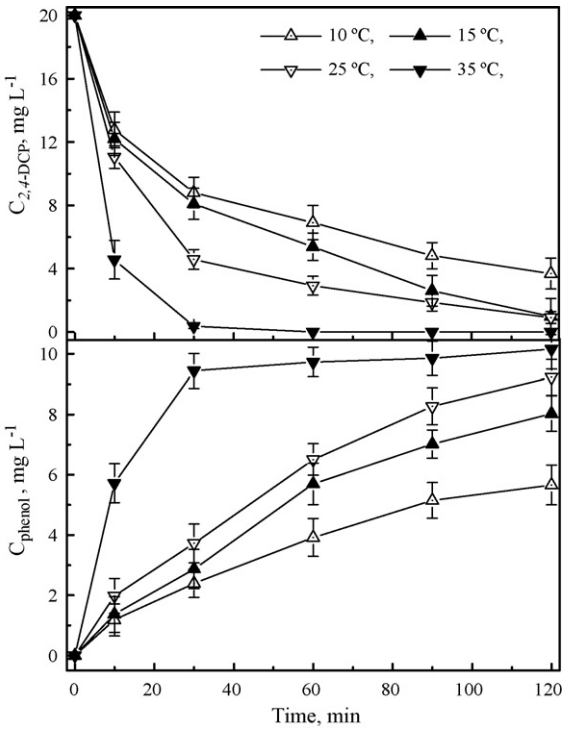

Fig. 9. Effect of temperature on 2,4-DCP dechlorination in the presence of humic acid (pH_{in}: 5.7, $C_{2,4\text{-DCP}}$: 20 mg L^{-1}, C_{HA}: 10 mg L^{-1}, $C_{Ni\text{-}Fe}$: 6 g L^{-1}, stirring at 400 rpm, the nickel content was 2.0 wt%).

3.7. Temperature effect on degree of dechlorination in the presence of HA

The temperature effect on the degradation of 2,4-DCP was also studied. The solutions were incubated at different temperatures (namely, 10, 15, 25 and 35 °C) for 10 min before reactions, followed by addition of HA and 2,4-DCP at constant temperatures. Fig. 9 shows the effect of temperature on the dechlorination of 2,4-DCP in the presence of HA. The degradation and dechlorination efficiency of 2,4-DCP and the production rates of phenol increased dramatically with the increase of the temperature. With the temperature increasing from 10 to 35 °C, the final removal percentage of 2,4-DCP increased from 82% to 100%, meanwhile the formed phenol increased from 5.66 to 10.16 mg L^{-1} in 2 h. At 10 °C, the dechlorination of 2,4-DCP was incomplete, the final removal percentage of 2,4-DCP only reached 82% after 2 h of reaction. When the temperature was 25 °C, 2,4-DCP could be nearly completely reduced to phenol. At 35 °C 2,4-DCP dechlorination becomes much faster possibly due to that the mobility of 2,4-DCP from solution to nanoparticles increased at higher temperature, or the activation energy for electron transfer or formation of a reactive surface complex increased. Based on these results, the remaining experiments were performed at a mixing temperature of 25 °C.

3.8. Characterization of nanoscale Ni–Fe particles

Fresh nanoscale Ni–Fe shows black and floccule. Since the size of nanoscale particles is smaller than the wavelength of visible light, they display perfect black body for light absorbance. Fig. 10 shows the TEM images of (a) fresh synthesized nanoscale Ni–Fe particles, (b) nanoscale Ni–Fe particles in HA solution for 2 h, (c) nanoscale Ni–Fe particles after 2 h of reaction. The particles are spherical with the sizes ranging from 20 to 100 nm in diameter. Spherical particles aggregate to form dendrites due to geomagnetic forces between nanoscale particles and small particles, and their surface tension interactions. A mucous layer was adhered onto the surface of Ni–Fe in HA solution for 2 h, reflecting the possibility of lowering the dechlorination efficiency. A more thicker mucous layer was showed on the surface of the nanoscale Ni–Fe particles after 2 h of reaction (Fig. 10(c)). More organic components such as HA and 2,4-DCP, as well as metal hydroxides and carbonate passivating layers on the nanoparticles' surface inhibited the particles' active sites, likely leading to lower dechlorination efficiency.

3.9. Mechanisms and kinetics for aqueous-phase dechlorination of 2,4-DCP with freshly synthesized Ni–Fe nanoparticles

The chlorinated compounds adsorbed on the nanoparticles surface were reductively dechlorinated through a series of reactions. The current model for the dehalogenation reaction using Ni–Fe nanoparticles involved the oxidation of iron to galvanically protected Ni [11]. As iron corrodes, protons from solution were reduced to atomic and molecular hydrogen at the catalytic Ni surface. Chlorinated compounds were also adsorbed on the surface of Ni–Fe particles where the C–Cl bond was broken, and the chlorine atom was replaces by hydrogen. The chemical progress can be represented as follows:

Surface reaction:

$$Fe + 2H^+ \rightarrow Fe^{2+} + H_2 \quad (3)$$

$$Fe + 2H_2O \rightarrow Fe^{2+} + H_2 + 2OH^- \quad (4)$$

$$H^+ + e \xrightarrow{Ni(Pd)} H* \quad (5)$$

Dechlorination reaction:

$$H* + 2,4\text{-DCP} \xrightarrow{Ni(Pd)} CP + Cl^- \quad (6)$$

$$H* + CP \xrightarrow{Ni(Pd)} P + Cl^- \quad (7)$$

Ferrous ions then react with dissolved oxygen and hydroxyl generated from water, or react with hydroxyl and carbonate, forming surface passivating layers on the surface of the nanoparticles, blocking further reaction. Presumably, the iron corrosion is the rate limited reaction under the experimental condition of the present study. Therefore, detection of ferrous ions and total iron ions produced in the reaction, which were shown in Fig. 3, also the elevation of solution pH during the reaction (Fig. 5), could support our assumption.

The overall dechlorination reaction takes place on the nanoparticles catalyst surface can be represented as

$$Fe^0 + 2,4\text{-DCP} + 2H* \rightarrow P + Fe^{2+} + 2Cl^- \quad (8)$$

At low pH, more atomic hydrogen on the catalyst surface attacked 2,4-DCP to replace the chlorine and to form CP, phenol and chlorine ion (Eqs. (6)–(8)). Meanwhile, surface passivating layers due to the precipitation of metal hydroxides and metal carbonates, which were developed at higher pH values, might not be easily formed at lower pH, would block the corrosion of iron, finally led the reduction of the 2,4-DCP dechlorination efficiency.

Fig. 11 shows the mechanisms of 2,4-DCP dechlorination by Ni–Fe nanoparticles in the presence of humic acid before and after the reaction, It is hypothesized that the existence of specific active surface sites designated for 2,4-DCP reduction, not for HA adsorption. But in the presence of HA, HA would compete active surface sites with 2,4-DCP. With the reactions proceeding to exhaust those specific sites, the common active sites available for both 2,4-DCP reduction and HA adsorption become limited. The adsorption of HA, together with the precipitation of metal hydroxides and metal carbonates on the nanoparticles, occupy the active surface sites and

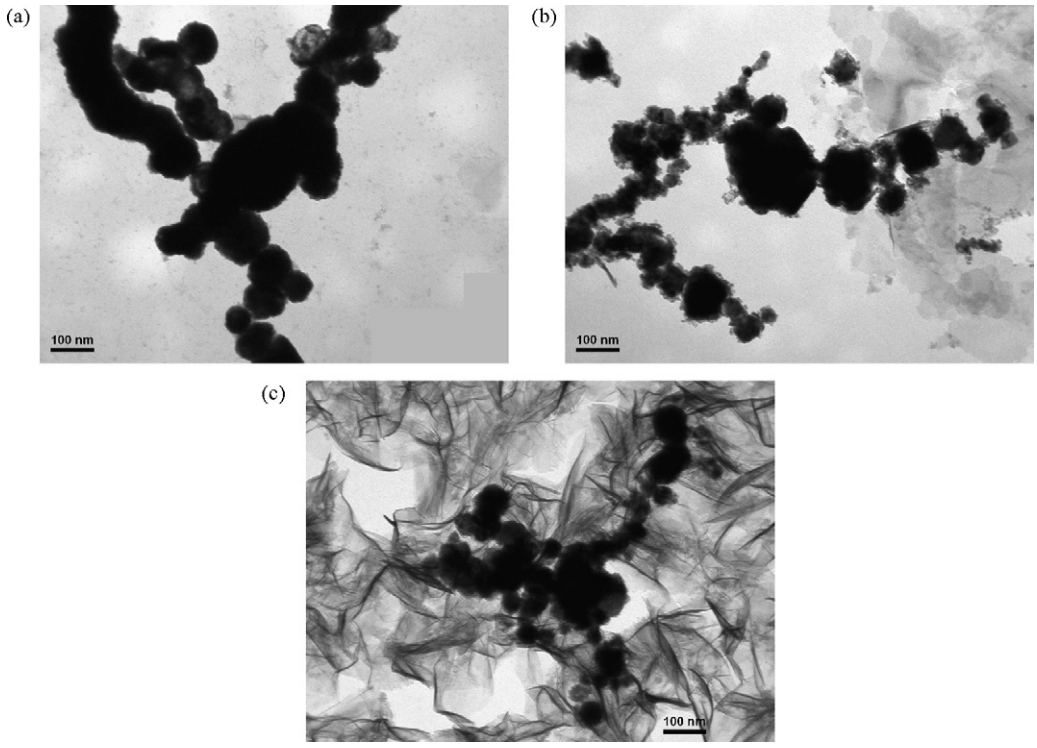

Fig. 10. TEM images of (a) fresh synthesized Ni–Fe nanoparticles, (b) nanoscale Ni–Fe particles in HA solution for 2 h, and (c) nanoscale Ni–Fe particles after 2 h of reaction.

inhibit iron corrosion, leading to the further decrease of the 2,4-DCP dechlorination efficiency.

Previous studies have shown that the degradation rate of chlorinated solvents by Ni–Fe nanoparticles follows a pseudo-first-order reaction, if the dosage of Ni–Fe nanoparticles is excessive in the reaction [5,14,30]. Chlorines of 2,4-DCP might be removed from the benzene ring following a stepwise (2,4-DCP → CP → P) pathway shown as below:

$$2,4\text{-DCP} \xrightarrow{k_1} \text{CP} + \text{Cl} \xrightarrow{k_2} \text{P} + 2\text{Cl} \tag{9}$$

where CP represents the total mol of *o*-CP and *p*-CP in the reaction. k_1 and k_2 refer the corresponding reaction rate for the disappearance of 2,4-DCP and CP. The corresponding reaction rate equations for the disappearance of 2,4-DCP, the transient formation of CP intermediate, and the accumulation of P in the batch system are as follows:

$$\frac{-dC_{2,4\text{-DCP}}}{dt} = k_1 C_{2,4\text{-DCP}} \tag{10}$$

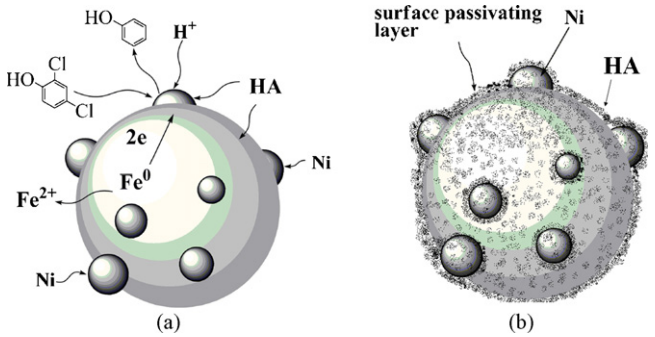

Fig. 11. The mechanisms of 2,4-DCP dechlorination by Ni–Fe in the presence of humic acid (a) reaction, (b) after reaction.

$$\frac{dC_{CP}}{dt} = k_1 C_{2,4\text{-DCP}} - k_2 C_{CP} \tag{11}$$

$$\frac{d[P]}{dt} = k_2 C_{CP} \tag{12}$$

The above simultaneous rate equations are solved, leading to the following molar fractions:

$$\alpha_{2,4\text{-DCP}} = e^{-k_1 t} \tag{13}$$

$$\alpha_{CP} = \frac{k_1}{k_2 - k_1}(e^{-k_1 t} - e^{-k_2 t}) \tag{14}$$

$$\alpha_P = 1 - \alpha_{2,4\text{-DCP}} - \alpha_{CP} \tag{15}$$

where α represents molar fraction of the subscript compound to the initial concentration of parent compound (i.e., 2,4-DCP). Since a fraction of organic compounds were absorbed by the Ni–Fe nanoparticles on their large surface area, the concentration of organic compound in aqueous-phase has to be revised. As the production of P was stepwise, equilibrium time required for organic compounds absorption onto Ni–Fe nanoparticles was little, and the total molar fraction of the organic compounds did not change, the proportion of P in aqueous-phase can be seen as invariable, and Eq. (15) can be revised as following:

$$\alpha'_P = \alpha_P \times (1 - a) \tag{16}$$

where a represents the molar fraction of the organic compounds which were adsorbed onto Ni–Fe nanoparticles to the initial concentration of parent compound (i.e., 2,4-DCP). Then k values were derived from fitting the experimental data into Eq. (16) according to the non-linear least-square regression.

k values in different reaction conditions were listed in Table 1. It shows that k values for 2,4-DCP dechlorination dropped from 0.14, 0.051, 0.039, 0.021 to 0.011 min^{-1} with the increasing HA concentrations from 0, 5, 10, 30 to 40 $mg\,L^{-1}$. And they increased obviously from 0.0054, 0.0080, 0.011, 0.033, 0.044 to 0.049 min^{-1} as the nickel content increased from 0.5, 0.75, 1.0,

Table 1
k values in different experimental conditions.

Reaction conditions		$1-\alpha$	k_1	R	k_2	R
2,4-DCP concentration	10 mg L^{-1}	0.88	0.11	0.998	0.34	0.976
	20 mg L^{-1}	0.93	0.044	0.991	0.028	0.990
	30 mg L^{-1}	0.91	0.058	0.992	0.085	0.992
	40 mg L^{-1}	0.97	0.050	0.999	0.037	0.992
	50 mg L^{-1}	0.92	0.045	0.999	0.064	0.994
	60 mg L^{-1}	0.92	0.053	0.995	0.081	0.994
Ni–Fe dosage	4 g L^{-1}	0.94	0.018	0.999	0.016	0.971
	6 g L^{-1}	0.92	0.043	0.991	0.028	0.990
	8 g L^{-1}	0.86	0.087	0.975	0.036	0.993
Temperature	15 °C	0.89	0.024	0.988	0.035	0.990
	25 °C	0.92	0.04	0.991	0.028	0.990
	35 °C	0.90	0.14	0.999	0.25	0.999
pH values	3.0	0.84	0.45	0.961	0.064	0.960
	6.0	0.92	0.043	0.991	0.028	0.990
	8.0	0.97	0.0066	0.946	0.023	0.990
	9.0	0.95	0.0042	0.977	0.031	0.988
Ni ratio in Ni–Fe	0.5%	0.98	0.0054	0.990	0.0068	0.949
	0.75%	0.94	0.0080	0.984	0.012	0.978
	1.0%	0.95	0.011	0.988	0.017	0.968
	1.5%	0.86	0.033	0.989	0.039	0.989
	2.0%	0.93	0.044	0.991	0.028	0.990
	3.0%	0.93	0.049	0.991	0.025	0.991
HA dosage	0 mg L^{-1}	0.86	0.14	0.999	0.28	0.997
	5 mg L^{-1}	0.84	0.051	0.959	0.19	0.995
	10 mg L^{-1}	0.94	0.039	0.997	0.029	0.990
	30 mg L^{-1}	0.98	0.021	0.975	0.015	0.943
	40 mg L^{-1}	0.90	0.011	0.979	0.011	0.890

Note: $1-\alpha$ represents the molar fraction of the total organic compounds in solution; k_1 and k_2 refer the corresponding reaction rate for the disappearance of 2,4-DCP and CP, respectively; R denotes the correlation coefficient between the experimental data can match the calculated number.

1.5, 2.0 to 3.0 wt%. In short, *k* values increased with the increasing addition of Ni–Fe nanoparticles, Ni loading percentage over Fe and temperature, with the decrease of pH values and HA dosage, and *k* values have nothing to do with the initial 2,4-DCP concentration.

In natural environments, humic susbtances were commonly found in groundwater, they are abundant and play important roles in adsorption processes. It is worthy of further investigation to find the possible remedy for humic acid before using Ni–Fe nanoparticles for the in situ remediation of contaminated groundwater. Some evidence show that carboxymethyl cellulose (CMC) stabilized Fe nanoparticles were the possible remedy for humic acid in the remediation of Cr(VI) contaminated water. Whether carboxymethyl cellulose (CMC) stabilized Ni–Fe nanoparticles can eliminate the HA's inhibitory effect on 2,4-DCP dechlorination or not need further investigation.

4. Conclusion

Our experimental results suggest that HA has an inhibitory effect on 2,4-DCP dechlorination, especially in low concentrations. In the dechlorination of chlorinated hydrocarbons, HA could act as an adsorbate competing reactive sites on the surface of Ni–Fe nanoparticles which led to a decrease in the dechlorination rate. The concentrations of HA in groundwater usually vary in different areas. It is of great importance to clarify the inhibitory effects of HA on 2,4-DCP dechlorination rates and establish appropriate conditions in the dechlorination of chlorinated hydrocarbons in order to reduce those inhibitory effects.

Acknowledgements

The authors are grateful for the financial support provided by the National Natural Science Foundation of China (No. 20407015) and the Program for New Century Excellent Talents in Universities (No. NCET-06-0525).

References

[1] A.A. Meharg, J. Wright, D. Osborn, Chlorobenzenes in rivers draining industrial catchments, Sci. Total Environ. 251 (251) (2000) 243–253.
[2] H. Wang, J.L. Wang, Electrochemical degradation of 4-chlorophenol using a novel Pd/C gas-diffusion electrode, Appl. Catal. B 77 (2007) 58–65.
[3] R.P. Schwarzenbach, E. Molnar-Kubica, W. Giger, S.G. Wakeham, Distribution, residence time, and fluxes of tetrachloroethylene and 1,4-dichlorobenzene in Lake Zurich, Switzerland, Environ. Sci. Technol. 13 (1979) 2154–2156.
[4] B.G. Oliver, K.D. Nicol, Chlorobenzenes in sediments, water, and selected fish from Lakes Superior, Huron, Erie, and Ontario, Environ. Sci. Technol. 16 (1982) 532–536.
[5] B.W. Zhu, T.T. Lim, J. Feng, Reductive dechlorination of 1,2,4-trichlorobenzene with palladized nanoscale Fe^0 particles supported on chitosan and silica, Chemosphere 65 (2006) 1137–1146.
[6] H.L. Lien, W.X. Zhang, Nanoscale Pd/Fe bimetallic particles: catalytic effects of palladium on hydrodechlorination, Appl. Catal. B 77 (2007) 110–116.
[7] Y. Fang, S.R. Al-Abed, Dechlorination kinetics of monochlorobiphenyls by Fe/Pd: effects of solvent, temperature, and PCB concentration, Appl. Catal. B 78 (2007) 371–380.
[8] W.X. Zhang, C.B. Wang, H.L. Lien, Treatment of chlorinated organic contaminants with nanoscale bimetallic particles, Catal. Today 40 (1998) 387–395.
[9] S.F. Cheng, S.C. Wu, The enhancement methods for the degradation of TCE by zero-valent metals, Chemosphere 41 (2000) 1263–1270.
[10] F. Li, C. Vipulanandan, K.K. Mohanty, Microemulsion and solution approaches to nanoparticle iron production for degradation of trichloroethylene, Colloid Surf. A 233 (2003) 103–112.
[11] B. Schrick, J.L. Blough, A.D. Jones, T.E. Mallouk, Hydrodechlorination of trichloroethylene to hydrocarbons using bimetallic nickel–iron nanoparticles, Chem. Mater. 14 (2002) 5140–5147.
[12] L.F. Wu, S.M.C. Ritchie, Removal of trichloroethylene from water by cellulose acetate supported bimetallic Ni/Fe nanoparticles, Chemosphere 63 (2006) 285–292.
[13] F. He, D. Zhao, Preparation and characterization of a new class of starch-stabilized bimetallic nanoparticles for degradation of chlorinated hydrocarbons in water, Environ. Sci. Technol. 39 (2005) 3314–3320.
[14] X.H. Xu, H.Y. Zhou, P. He, D.H. Wang, Catalytic dechlorination kinetics of *p*-dichlorobenzene over Pd/Fe catalysts, Chemosphere 58 (2005) 1135–1140.
[15] X.H. Xu, H.Y. Zhou, D.H. Wang, Structure relationship for catalytic dechlorination rate of dichlorobenzenes in water, Chemosphere 58 (2005) 1497–1502.
[16] X.H. Xu, H.Y. Zhou, M. Zhou, Catalytic amination and dechlorination of para-nitrochlorobenzene (*p*-NCB) in water over palladium–iron bimetallic catalyst, Chemosphere 62 (2006) 847–852.
[17] S.F. Cheng, S.C. Wu, Feasibility of using metals to remediate water containing TCE, Chemosphere 43 (2001) 1023–1028.
[18] B. Coq, F. Figueras, Bimetallic palladium catalysts: influence of the co-metal on the catalyst performance, J. Mol. Catal. A: Chem. 173 (2001) 117–134.
[19] H.L. Lien, W.X. Zhang, Nanoscale iron particles for complete reduction of chlorinated ethenes, Colloid Surf. A. 233 (2001) 103–112.
[20] T.L. Johnson, W. Fish, Y.A. Gorby, P.G. Tratnyek, Degradation of carbon tetrachloride by iron metal: complexation effects on the oxide surface, J. Contam. Hydrol. 29 (1998) 379–398.
[21] P.G. Tratnyek, M.M. Schere, S. Hu, Effects of natural organic matter anthropogenic surfactants, and model quinones on the reduction of contaminants by zerovalent iron, Water Res. 35 (2001) 4435–4443.
[22] G.P. Curtis, M. Reinhard, Reductive dehalogenation of hexachloroethane, carbon tetrachloride, and bromoform by anthrahydroquinone disulfate and humic acid, Environ. Sci. Technol. 28 (1994) 2393–2401.
[23] D.R. Lovley, J.D. Coates, E.L. Blunt-Harris, E.J.P. Phillips, J.C. Woodward, Humic substances as electron acceptors for microbial respiration, Nature 382 (1996) 445–448.
[24] R.A. Doong, Y.J. Lai, Dechlorination of tetrachloroethylene by palladized iron in the presence of humic acid, Water Res. 39 (2005) 2309–2318.
[25] E. Sahinkaya, F.B. Dilek, Biodegradation of 4-CP and 2,4-DCP mixture in a rotating biological contactor (RBC), Biochem. Eng. J. 31 (2006) 141–147.
[26] D.R. Burris, T.J. Campbell, V.S. Manoranjan, Sorption of trichloroethylene and etrachloroethylene in a batch reactive metallic iron–water system, Environ. Sci. Technol. 29 (1995) 2850–2855.
[27] L. Xie, C. Shang, Role of humic acid and quinone model compounds in bromate reduction by zerovalent iron, Environ. Sci. Technol. 39 (2005) 1092–1100.
[28] M.C. Lu, J. Anotai, C.H. Liao, W.P. Ting, Dechlorination of hexachlorobenzene by zero-valent iron, Pract. Periodical Hazard. Toxic Radioact. Waste Manage. 8 (2004) 136–140.

[29] H. Song, E.R. Carraway, Reduction of chlorinated ethanes by nanosized zero-valent iron: kinetics, pathways, and effects of reaction conditions, Environ. Sci. Technol. 39 (2005) 6237–6245.
[30] Y. Fang, S.R. Al-Abed, Dechlorination kinetics of monochlorobiphenyls by Fe/Pd: effects of solvent, temperature, and PCB concentration, Appl. Catal. B 78 (2008) 371–380.
[31] G.N. Jovanovic, P. Plazl, P. Sakrittichai, K. Al-Khald, Dechlorination of p-chlorophenol in a microreactor with bimetallic Pb/Fe catalyst, Ind. Eng. Chem. Res. 44 (2005) 5099–5106.
[32] J.T. Nurmi, P.G. Tratnyek, V. Sarathy, D.R. Baer, J.E. Amonette, K. Pecher, C.M. Wang, J.C. Linehan, D.W. Matson, R.L. Penn, M.D. Driessen, Characterization and properties of metallic iron nanoparticles: spectroscopy, electrochemistry, and kinetics, Environ. Sci. Technol. 39 (2005) 1221–1230.
[33] Y.H. Kim, E.R. Carraway, Dechlorination of pentachloropenol by zero valent iron and modified zero valent irons, Environ. Sci. Technol. 34 (2000) 2014–2017.
[34] Y. Liu, G.V. Lowry, Effect of particle age (Fe^0 content) and solution pH on NZVI reactivity: H_2 evolution and TCE dechlorination, Environ. Sci. Technol. 40 (2006) 6085–6090.